Simulations of Bragg diffraction of a focused x-ray beam by a single crystal with an epitaxial layer

V. G. Kohn[1,*] and A. Kazimirov[2,†]

[1]*Russian Research Center "Kurchatov Institute," 123182, Moscow, Russia*
[2]*Cornell High Energy Synchrotron Source, Cornell University, Ithaca, New York 14853, USA*

The Bragg case diffraction of a narrow x-ray beam in a multilayer crystal is studied theoretically. The beam produced by a parabolic refractive lens is Bragg reflected by a crystalline sample and a spatial distribution of the intensity is recorded by a detector placed at the focus of the lens. This x-ray optical scheme represents a topographic technique which is extremely sensitive to a depth variation of a crystalline structure. Simulations of the intensity pattern were performed by using a computational technique based on a convolution of individual propagators by performing a double fast Fourier transform procedure. It was shown that each interface in a multilayer crystal can be observed on the intensity pattern with a contrast depending on the incident angle. Thus, by recording a series of images at different angles, valuable depth sensitive structural information can be obtained.

I. INTRODUCTION

X-ray diffraction is a powerful tool to study the atomic structure of crystals, surface layers, and interfaces. High-resolution diffractometry is based on using a well collimated x-ray beam, which can be approximated by a plane wave, and recording the angular dependence of the diffracted intensity (rocking curve). X-ray rocking curve can provide direct information about lattice constant changes and lattice perfection integrated over the surface area of the beam footprint. Depth information can only be obtained through computer simulation by fitting rocking curve to a theoretical model. Information about the location of a crystal defect or distorted region inside a crystalline volume can be obtained by using x-ray topographic technique such as x-ray section topography, which is based on using a very narrow x-ray beam and a two-dimensional x-ray detector (see, e.g., Ref. 1, and references there). Such a narrow beam is usually prepared by a slit with a width of about 10 μm placed in front of the sample. This technique is well suited for the Laue case of diffraction in which the diffracted beam propagates through the bulk and the image is registered at the exit surface of the crystal. It has been successfully developed over the decades into an established technique demonstrating excellent agreement between experimental and computer simulated images of crystal defects.

A general theory of diffraction of a spatially heterogeneous x-ray beam in the Bragg case was developed in the early 1970s. An analytical formula was derived by several groups[2–4] for the amplitude of the diffracted wave as a function of the coordinate along the exit surface (which is, for the Bragg case, also the entrance surface) in the case of an incident spherical wave from the point source located on the entrance surface. This function, being per se the propagator of the crystal, allows one to calculate the amplitude of coherently reflected wave in the case of arbitrary incident wave by means of convolution. The propagator was calculated as a solution of the Takagi equations[2,3] as well as by a direct integration of the amplitude of the reflected plane wave over the total angular region near the Bragg angle[4] which is equivalent to the Fourier transformation.

Analytical solution for the propagator obtained for the crystal of finite thickness[2–4] revealed an interesting physical phenomenon: a strong reflection is created not only from the front (entrance) surface but also from the back surface of a crystalline slab. In analogy with reflection of acoustic waves we may call this an "echo." Analytical expression for the reflection from the back surface was derived in Ref. 3 in the form of Bessel functions and it shows a very strong peak with intensity decreasing only on the path from the entrance to exit and back to entrance surfaces due to a normal absorption. The phenomenon of the strong reflection from the back surface is in apparent contradiction with the well known extinction effect, i.e., a small penetration depth inside the crystal of the plane wave entering the crystal at an angle corresponding to the center of the total reflection region. Though the detailed theoretical analysis of this phenomenon is still missing, the physical explanation can be sought for in the fact that diffraction of a very narrow beam or a spherical wave from the source located close to the surface can be considered as a coherent superposition over all angles including slowly decreasing "tails" of the angular rocking curve. These kinematical tails form the maximum of the reflected wave at the point of entrance of the narrow beam into the crystal. In a multilayer crystal, due to the kinematical nature of this phenomenon strong reflection should take place at each interface.

In contrast to the Laue case, in the Bragg case the propagator, to the best of our knowledge, has never been measured and the phenomenon described above has never been observed experimentally. The reason is quite simple: any slit placed in front of the crystal would inevitably block the diffracted beam and not allow any accurate quantitative measurements. X-ray topography analysis in the Bragg case is usually based on a Berg-Barrett technique (see details in Ref. 1) in which a narrow beam is incident on a crystal surface at a glancing angle and diffraction image is registered on a film placed parallel to the surface. While yielding useful qualitative information about the perfection of the surface layer this setup cannot reproduce conditions of the theoretical description and therefore does not allow direct comparison with
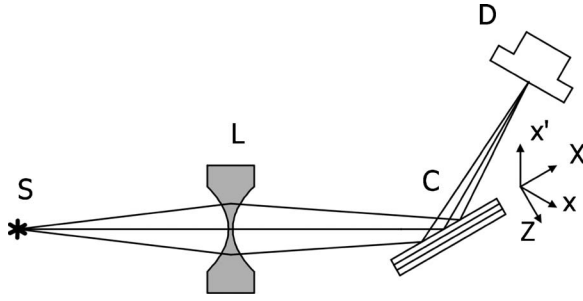
FIG. 1. X-ray optical scheme of a numerical experiment. S: a point source of x rays, L: a parabolic x-ray lens, C: a multilayer crystal, D: a position sensitive detector. The axis x' is perpendicular to the direction of the incident beam and the axis x is perpendicular to the direction of the diffracted beam; both are in the diffraction plane (the plane of figure). The axes X and Z are referred to the crystal.

theory. In this work we propose a experimental approach based on using a focused x-ray beam.

Last decade witnessed remarkable progress in x-ray focusing optics. Eleven years ago x-ray compound refractive lenses (CRLs) were proposed[5] which are now under extensive development. For the purpose of this work the parabolic CRL (Ref. [6]) has certain advantages over other types of focusing optics. First, it produces a clean focus without aberrations. Since we are interested in two-beam Bragg diffraction the planar CRL (Ref. [7]) which focuses waves only in one plane, the diffraction plane in our case, is sufficient. Second, since under the symmetrical diffraction the crystal does not change the width of the beam the intensity distribution does not depend on the specific position of the crystal between the lens and the detector. This allows one to place the x-ray detector at the focus and the crystal anywhere between the lens and detector. The recorded image will be exactly the same as when both crystal and detector are placed in the focus, a situation which is difficult to achieve in a real experiment. Preliminary analysis[8] performed on an x-ray Farby-Perot interferometer[9] confirms this conclusion.

In this work we present theoretical analysis and computer simulation of the experiment performed using this arrangement. The article is organized as follows. In Sec. II the theory and details of the computer simulation are presented. In Sec. III we describe diffraction by a single layer, compare computer simulations with calculations based on analytical formulas, and perform an estimation of the accuracy of the computer model. A more realistic case of two crystal layers, that can model a thick crystal with an epitaxially grown layer, will be described in Sec. IV, followed by a discussion and conclusion section.

II. THEORY AND METHOD OF COMPUTER SIMULATION

An x-ray optical scheme of a numerical experiment is shown in Fig. 1. A point source of x rays (S) creates a divergent spherical wave which propagates through an x-ray parabolic lens (L), reflects from a crystal (C) positioned between the lens and the focus, and the intensity distribution is regis-

tered by a position sensitive detector (D). The parabolic lens is considered in a thin lens approximation and positioned at a distance L_s from the source. It focuses the wave at the distance of $L_f = F/(1 - F/L_s)$ from the lens, where F is the focal length of the lens. The multilayered crystal is placed on the optical axis behind the lens and the detector is placed at a distance of L_f from the lens, i.e., in the lens focus. In Fig. 1, the z axis is along the optical axis, the transverse x axis is in the diffraction plane, i.e., in the plane of the figure, and the y axis is perpendicular to the diffraction plane.

Diffraction changes the spatial distribution of the wave field in the diffraction plane. The direction of the optical axis is rotated due to diffraction by an angle of $2\theta_B$, where θ_B is the Bragg angle. We use a paraxial approximation which is applicable for x rays with high accuracy. In this approximation, the Kirchhoff propagator $P(x, x', y, y', z)$ can be considered as a product of two functions, the first one describing the propagation in a y, z plane and the second one in a x, z plane, i.e., in a diffraction plane

$$P(x, x', y, y', z) = P(x, x', z)P(y, y'z), \quad (1)$$

where

$$P(x, x', z) = \frac{1}{(i\lambda z)^{1/2}} \exp\left(i\pi \frac{(x - x')^2}{\lambda z}\right) \quad (2)$$

describes the propagation of a transverse x component of the wave field in empty space along the optical axis z, λ is the wavelength. The goal of our analysis is to study how the transverse distribution of the wave field changes as the wave moves along the optical axis. We will consider a scalar amplitude of the radiation assuming that it is polarized normally to the scattering plane, as in the case of synchrotron radiation, therefore the polarization state is not important. Since the crystal effects the propagation of x rays in a diffraction plane only, it will be sufficient to analyze only the (x, z) dependence.

If the transverse dependence of the wave field $A(x)$ is known at a certain point on the optical axis, then the transfer of this field by a distance L is defined by a convolution of this field with the propagator $P(x, x', L)$. Because a point source can be approximated by the δ function, at a distance L from the source the amplitude of the radiation originated from the point source is equal to $P(x, 0, L)$. We will consider an x-ray lens as a thin object which disturbs the wave field according to the geometrical optics law (the peculiarities arising from the finite length of the lens can be taken into account by using an analytical expression for the propagator derived in Ref. [10], however, for our discussion they are not important). The propagator of the parabolic refractive lens does not depend on z and it can be written as

$$P_{PRL}(x, x') = T_{PRL}(x)\delta(x - x'), \quad (3)$$

where

$$T_{PRL}(x) = \exp\left(-i\pi \frac{x^2}{\lambda F}[1 - i\gamma]\right). \quad (4)$$

Here $\delta(x)$ is the Dirac delta function, $\gamma = \beta/\delta$, the parameters δ and β are the decrement of the refractive index and the

absorption index correspondingly, the mean susceptibility of the crystal $\chi_0 = -2\delta + i2\beta$, $F = R/2\delta$ is the focal length of the lens, and R is the effective radius of curvature. As it follows from Eq. (3), the lens changes the wave field locally at each point by the means of the transparent function $T_{PRL}(x)$. The real geometric aperture of the lens is not essential if the effective aperture, defined by the absorption, is much smaller than the real aperture, the case we will consider in our analysis.

Next, let us consider a propagator $P_{MC}(x, x')$ of the diffraction reflection of the beam by a multilayered crystal. It also does not depend on z and in the case of a symmetrical diffraction it is a function of the difference $(x - x')$. In this term the coordinate x is normal to the optical axis after the crystal, where the optical axis is rotated by the angle of $2\theta_B$, whereas the coordinate x' is normal to the initial optical axis before the crystal, as shown in the Fig. 1. There is also a coordinate system (X, Z) relative to the crystal: the Z axis is normal to the crystal surface and directed toward the interior of the crystal and the X axis is along the surface of the crystal in the diffraction plane. We assume that the crystal is uniform along the X axis. The propagator $P_{MC}(x, x')$ can be defined by means of the Fourier integral

$$P_{MC}(x, x') = \int \frac{dq}{2\pi} \widetilde{P}_{MC}(q) \exp[iq(x - x')]. \quad (5)$$

The function $\widetilde{P}_{MC}(q)$ is the reflection amplitude for the plane wave. It depends on the angular deviation (q/K) of the direction of the plane wave from the Bragg angle, $K = 2\pi/\lambda$. This function for the multilayered crystal has no analytical expression and must be calculated by means of recurrent relation which was derived in many works. Below we present it in the form which was obtained in Ref. 11. According to the treatment in Ref. 11, $\widetilde{P}_{MC}(q) = R_N(q)$, where N is the total number of layers in the multilayered system in which layers are numbered from the bottom (layer with the index 1, usually a substrate) to the top (layer with the index N). This result was obtained by the successive application of the recurrent formula

$$R_k(q) = \frac{R_1 - R_2 C \exp(i\varphi)}{1 - C \exp(i\varphi)}, \quad C = \frac{R_1 - R_{k-1}(q)}{R_2 - R_{k-1}(q)}, \quad (6)$$

$$\varphi = \frac{a d_L}{\gamma_0}, \quad a = (\sigma^2 - s^2 f)^{1/2}, \quad R_{1,2} = \frac{\sigma \pm a}{sf}, \quad (7)$$

$$\sigma = (q - q_0)\sin(2\theta_B) - i\mu_0, \quad s = K\chi_h, \quad (8)$$

$$f = \chi_{-h}/\chi_h, \quad \mu_0 = K\chi_0''. \quad (9)$$

Here the notation a'' means the imaginary part of a complex value a and it is assumed that $a'' > 0$. All parameters in Eqs. (6)–(9) refer to the kth layer. d_L is the layer thickness and χ_0, χ_h, χ_{-h} are the Fourier components of the susceptibility of the crystal lattice in the layer with the reciprocal lattice vectors **0**, **h**, and **−h**. We consider below the symmetrical case where $\gamma_0 = \sin\theta_B$. The parameter

$$q_0 = K\varphi + K[\Delta E/E + \Delta d/d]\tan\theta_B \quad (10)$$

describes deviation from the Bragg condition. Here, φ is a small angle of rotation of the crystal from the Bragg angle, $\Delta E/E$ is a relative change of the photon energy, and $\Delta d/d$ is a relative change of the crystal lattice d spacing for the reflecting atomic planes.

Generally speaking, the rotation of the crystal changes the direction of the output optical axis. In the case of fixed axis it can be taken into account by introducing an additional phase factor. In this work we assume that the crystal is fixed, i.e., $\varphi = 0$. The change of the energy $\Delta E/E$ can be used to account for the energy bandwidth of the incident radiation. By using the parameter $\Delta d/d$ a multilayer epitaxial structure in which each epitaxial layer may have a different lattice constant can be modeled.

Calculation of the space distribution of the radiation intensity at the detector position was performed by the means of a double fast Fourier transformation (FFT) technique according to the following scheme. The wave field just after the parabolic lens is $A(x) = P(x, 0, L_s)T_{PRL}(x)$. To take into account a transfer of the field on the distance L_1 between the lens and the crystal, we need to calculate a convolution of this function with the Kirchhoff propagator (2). We will apply the general property of the Fourier transformation, i.e., the Fourier image of the convolution of two functions is a product of the Fourier images of these two functions. Therefore, we calculate the Fourier image $\widetilde{A}(q)$ of the function $A(x)$ and multiply it by the Fourier image of the Kirchhoff propagator $\widetilde{P}(q, L_1)$. The latter function has a simple analytical expression

$$\widetilde{P}(q, z) = \exp\left(iz\frac{q^2}{2K}\right). \quad (11)$$

In the same way, the crystal can be taken into account by simply adding a new multiplier, the Fourier image of the crystal propagator, namely, $\widetilde{P}_{MC}(q)$ [see Eq. (5)]. Finally, to take into account the field transfer on the distance L_2 between the crystal and the detector, we add a new multiplier $\widetilde{P}(q, L_2)$. Since $\widetilde{P}(q, L_1)$ and $\widetilde{P}(q, L_2)$ are both multipliers, it follows directly from Eq. (11) that

$$\widetilde{P}(q, L_1)\widetilde{P}(q, L_2) = \widetilde{P}(q, L_1 + L_2) = \widetilde{P}(q, L_t). \quad (12)$$

Therefore, the resulted intensity distribution on the detector depends only on the total distance from the lens to the detector $L_t = L_1 + L_2$. The specific position of the crystal between the lens and the detector is not important. Of course, this conclusion is valid only under the assumption that the layers composing the crystal are homogeneous along the surface of the crystal. The size of the region, where the parameters must be homogeneous, depends on the footprint of the x-ray beam on the crystal and the size of the crystal region reflecting the beam.

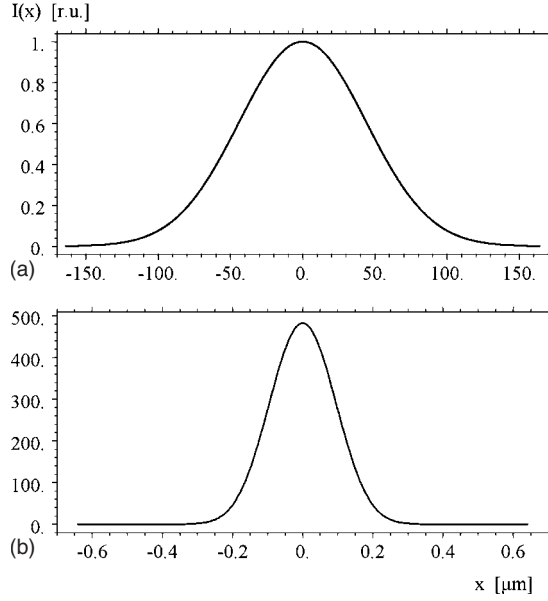Thus, we obtained the Fourier image of the field distribution at the detector as

FIG. 2. (a) Relative intensity distribution just behind the parabolic refractive lens. The FWHM of 104 μm is an effective aperture of the lens. (b) The relative intensity distribution at the focus of the lens. The FWHM is 0.22 μm which corresponds to the diffraction limit of the source.

$$\widetilde{B}(q) = \widetilde{A}(q)\widetilde{P}_{\mathrm{MC}}(q)\widetilde{P}(q,L_t), \tag{13}$$

The field $B(x)$ is calculated by using the inverse FFT procedure. The relative intensity distribution is defined as

$$I(x) = |B(x)|^2 \lambda (L_s + L_t). \tag{14}$$

To perform the calculations a computer program was written based on programming languages JAVA (Ref. 12) and ACL.[13] For the FFT procedure we used a set of $65\,536 = 2^{16}$ points with a step of 0.005 μm. The calculations were performed for the following parameters: the photon energy $E = 25$ keV, the source to lens distance $L_s = 50$ m, the aluminum parabolic lens with a focal length $F = 100$ cm, the effective curvature radius $R = 2\delta F = 1.729$ μm and the following values for the refraction parameters $\delta = 8.645 \times 10^{-07}, \beta = 1.761 \times 10^{-09}$ ($\gamma = \beta/\delta = 2.037 \times 10^{-03}$).

The calculated relative intensity distribution just after the lens is shown in Fig. 2(a). The curve has a Gaussian shape due to absorption within a parabolic thickness of the lens with a full width at half maximum (FWHM) of 104 μm. This value can be considered as an effective aperture A_γ of our particular lens and it agrees very well with the value calculated by using the following analytical formula:

$$A_\gamma = 0.664 \left(\frac{\lambda F}{\gamma} \right)^{1/2} \tag{15}$$

derived in Ref. 14. Figure 2(b) shows the relative intensity distribution at the distance of $L_f = 102$ cm, i.e., at the focus of the lens. The curve shows a maximum relative intensity of 490 and has a Gaussian shape with the FWHM of 0.22 μm which corresponds to the diffraction limit s_γ of the image of the source. Note that the Gaussian wave does not change its

shape in propagating through free space. The analytical formula[10]

$$s_\gamma = \gamma A_\gamma = 0.664(\lambda F \gamma)^{1/2} \tag{16}$$

gives a value of 0.21 μm which is close to what we obtained from the computer calculations (0.22 μm) and the small difference is partially due to the fact that the analytical formula was derived for the plane incident wave.

The important characteristic of the lens is the integrated over x relative intensity which can also be considered as an effective aperture. We obtain the value of 110 μm just after the lens and the same integrated intensity value at the focus distance (the last value was corrected by a geometrical factor $50/51$ to account for the difference in positions). Since there is no absorption in empty space both values must be equal.

III. DIFFRACTION BY ONE LAYER AND ESTIMATION OF ACCURACY

The propagator $P_{\mathrm{CP}}(x)$ of a single crystal plate of the thickness d in the Bragg case, i.e., a spatial distribution of the intensity of the reflected wave on the top surface of the crystal under illumination of the crystal by a very narrow beam (δ-functional source placed at $x = 0$ directly in front of the crystal) with the integral intensity of unity, was derived[2–4] in an analytical form thirty five years ago. Applying these formulas we can write the following expression for the intensity as a function of the coordinate x normal to the reflected beam in the case of symmetrical diffraction:

$$I_{\mathrm{CP}}(x) = \left| \frac{sF(x)}{2\sin(2\theta_B)} \right|^2 \exp\left(-\mu_0 \frac{2x}{\sin(2\theta_B)} \right), \tag{17}$$

$$F(x) = \theta(x)G_0(x) - \theta(x - x_0)G_1(x), \tag{18}$$

$$G_0(x) = J_0(Bx) + J_2(Bx), \tag{19}$$

$$G_1(x) = J_0(B\eta) + 2\xi J_2(B\eta) + \xi^2 J_4(B\eta), \tag{20}$$

$$B = \frac{(s^2 f)^{1/2}}{2\sin(2\theta_B)}, \quad x_0 = 2d\cos\theta_B, \tag{21}$$

$$\eta = (x^2 - x_0^2)^{1/2}, \quad \xi = \frac{x - x_0}{x + x_0}. \tag{22}$$

Here $J_n(x)$ is the Bessel function of the first kind and nth order, $\theta(x)$ is the Heaviside step function which is equal to unity for $x > 0$ and zero for $x < 0$, and other notations are defined by Eqs. (8) and (9).

We will consider the 111 reflection from the silicon crystal with the following diffraction parameters calculated based on a well known data: $\theta_B = 4.536°$, $\mu_0 = 5.016$ cm^{-1}, $s = (-1030.6 + i3.506)$ cm^{-1}, $f = 1$. The thickness of the crystal $d = 5$ μm and $x_0 = 9.969$ μm. The intensity distribution calculated with using Eqs. (17)–(22) is shown in Fig. 3(a). This intensity is measured in μm^{-1} and can be called the intensity density (ID). One can see that the ID maximum of 0.11 μm^{-1} is observed at the point of illumination and the

intensity decreases with x to the zero value at the distance of about 5 μm. However, at the point where the beam, reflected from the back surface of the crystal, reaches the front surface, i.e., at $x=x_0=9.969$ μm, the ID intensity shows a sharp peak with the intensity even slightly higher than at $x=0$. From the mathematical point of view, the reason for the second peak is that the function $G_0(x)$ at this point is not equal to zero but has a small negative value while the function $G_1(x)$ is equal to unity at this point. The second peak is very narrow and additional weak peaks can be observed in this region.

To understand this behavior better it is useful to discuss it in terms of the reflectivity amplitude for the plane wave. In the region just behind the point of illumination $x=0$ the crystal reflects the beam only within a thin layer near the top surface of the crystal (extinction length). In other words, the crystal plate of 5 μm thick works as an infinitely thick crystal. The reflectivity amplitude for the thick crystal has slowly decreasing angular tails so that $P_C(q) \approx s/2\sigma$ for $|\sigma/s| \gg 1$, where σ is defined by Eq. (8). Only these tails determine the behavior at $x=0$ and nearby region of small x. It is easy to verify this conclusion by applying Eq. (5) to the tails

$$P_C(x) = \frac{s}{2\sin(2\theta_B)} \int \frac{dq}{2\pi} \frac{\exp(iqx)}{[q - i\mu_0/\sin(2\theta_B)]}$$

$$= \frac{si}{2\sin(2\theta_B)} \theta(x) \exp\left(-\frac{\mu_0 x}{\sin(2\theta_B)}\right). \quad (23)$$

Therefore, the reflection of a very narrow beam by the perfect crystal is quite different from the reflection of a plane wave: the maximum intensity takes place under condition of the kinematical but not the dynamical diffraction. It is well known that the tails of the rocking curves (also known as crystal truncation rods) are very sensitive to the structure of a very thin surface layer.[15–17] We may expect therefore that the technique based on the reflection of a narrow beam may have very useful applications in the analysis of the surface layers.

The dynamical diffraction leads to the extension of the reflection region up to $x=5$ μm, i.e., to the broadening of the reflected beam. There is a weak additional maximum observed in this region which is due to the interference of the waves reflected from the different depths of the crystal. It is well known that the amplitude of the plane waves within the dynamical angular region decreases strongly with the depth and they are absent inside the bulk of the crystal. However, this is not the case for the kinematical angular region. The waves scattered by atoms from various depths of the crystal have various phases and the destructive interference of these waves leads to the absence of the reflection intensity. However, the incident beam is still present inside the crystal. The back surface of the crystal breaks the destructive interference and, as a result, the kinematical reflection becomes possible once again. The maximum intensity is high but it does not extend significantly since it is only due to the kinematical diffraction. A series of additional peaks with decreasing intensity can be observed in the region of $x > 10$ μm. The integrated over x intensity of the reflected beam is equal to 0.32. Therefore, 68% of the intensity passes through the crystal and exits through the back surface.
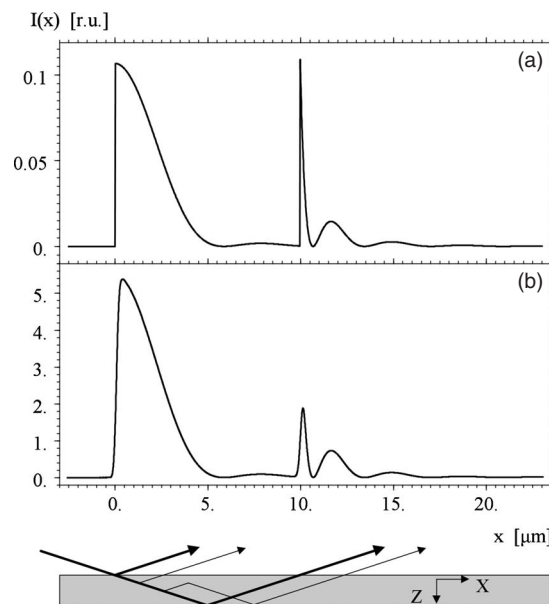

FIG. 3. (a) Spatial relative intensity distribution of the 111 Bragg reflected beam from a point source placed at the front surface of the 5 μm thick crystalline plate. Calculations were performed by using analytical expressions based on the Bessel functions. Computer simulation for the narrow slit with the opening of 0.01 μm and unit integral intensity incident on the crystal reproduce with high accuracy the analytical curve (see text for the details). (b) Spatial relative intensity distribution of the focused x-ray beam for the same conditions and at the focus of the parabolic refractive lens. The bottom panel shows the rays trajectories inside the crystal (see text for the details).

The bottom panel in Fig. 3 helps us to understand the calculated intensity distribution in terms of rays reflected from atomic planes. For illustrative purposes the Bragg angle was increased by a factor of 4. The ray trajectories are shown in the (X, Z) coordinates referred to the crystal (see Fig. 1) while the intensity pattern is calculated in the plane perpendicular to the reflected beam. In the kinematical approximation known also as the first Born approximation, only one reflection is taken into account and multiple reflections are neglected. The reflected beam is formed by a single reflection from the incident ray as shown by the top thin line. Dynamical diffraction theory considered here takes into account multiple reflections leading to the accurate solution for perfect crystals. Due to multiple reflections the rays can follow complicated trajectories before leaving the crystal as illustrated by the path shown by the bottom thin line. In particular, the multiple reflections are responsible for the nonzero reflected intensity in the region of $x > 10$ μm where a single reflection does not exist.

To estimate the accuracy of the computer simulation described in the previous section we performed calculation for the case where a very narrow slit with the opening of 0.01 μm was placed in front of the crystal. The integral intensity of the incident radiation was equal to unity. The result is very close to the analytical curve. The difference between the curve, obtained by using the Bessel functions, and the curve, obtained from the computer simulation, shows non-

zero values (less than 10%) only in very narrow regions near the sharp vertical edges due to a finite region of FFT calculation and the long tails of Fourier image of the narrow slit. Anywhere except these points the two curves coincide completely. We may conclude that for the real objects with shorter tails of Fourier image the accuracy of the computational method is acceptable. Note also that with the density of the incident intensity of 100 μm^{-1} the maximum of the reflected ID is close to 0.1 μm^{-1}, three orders of magnitude have been lost.

Next, let us again consider the setup in Fig. 1 and calculate the intensity distribution on the detector placed in the focus of the refractive lens at the distance of $L_t = L_f$ with the parameters of the lens the same as in the previous section. The crystal is placed in the path of the focused beam between the lens and the detector and the crystal parameters are the same as we used for the calculation with the narrow slit. As it follows from the previous discussion, we expect to see the distribution of the relative intensity close to the one obtained above for the narrow slit and the detector placed at the crystal surface. The result of the calculation is shown in Fig. 3(b). Indeed, the main features are the same as in Fig. 3(a) though the peaks are less sharp. That proves that the setup with the focused beam can be used to analyze the details of the spatial distribution of the reflected beam instead of the setup with the narrow slit which is not feasible in practice. It is of interest to note also that with the maximum intensity in the incident focused beam of 500 [Fig. 2(b)] the maximum intensity in the reflected beam is about 5, i.e., we have two orders of magnitude lost instead of three orders as in the case with the narrow slit.

IV. DIFFRACTION BY THICK CRYSTAL WITH ONE EPITAXIAL LAYER

In this section we will analyze a system with two layers, typically it is a thick substrate and one layer on top of it. For simplicity we assume that the material of both the substrate and the layer is silicon, the substrate is sufficiently thick with the thickness of 1 mm and, as in the previous sections, we consider the 111 reflection. The layer may have different lattice constant relative to the substrate. The experimental arrangement is as in Fig. 1: the beam, focused by the refractive parabolic lens with the same parameters as in the previous sections, is incident on the crystal at the angle close to the Bragg angle for the 111 reflection.

The spatial intensity distributions for the layer with a thickness of 2 μm and different d-spacing differences of $\Delta d / d = D \times 10^{-4}$ for $D = 0, 1, 2, 4, 10$ are shown in Fig. 4. The angular position of the sample corresponds to the Bragg angle for the substrate. The top curve for $D = 0$ shows one peak because the layer perfectly matches the substrate and the beam does not recognize it. This peak is described by the propagator for a thick crystal averaged over the resolution of the lens and the edge of the peak corresponds to the surface of the sample. However, even at $D = 1$ the second peak appears at $x = x_0 \simeq 4$ μm which corresponds to the reflection from the substrate. This peak is formed at the interface between the layer and the substrate and the physical reason for
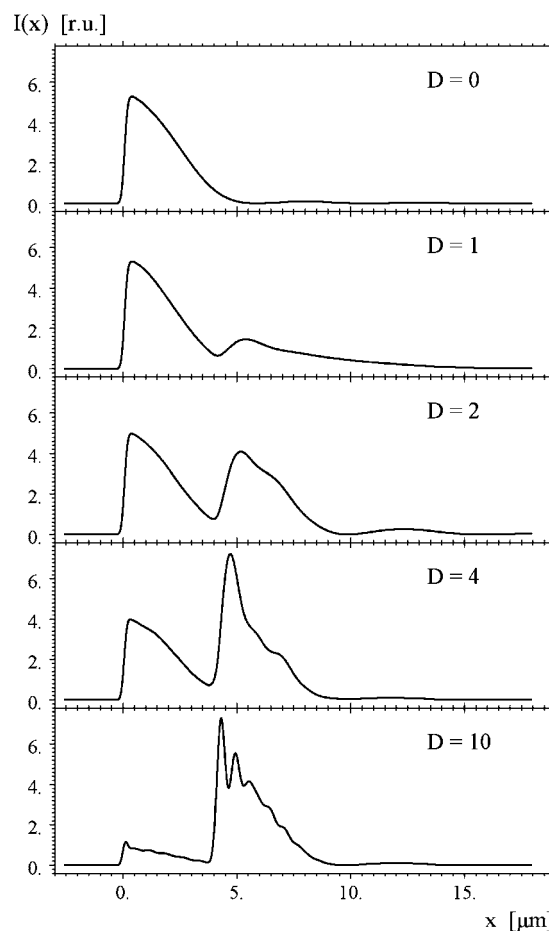

FIG. 4. Spatial relative intensity distribution of a focused beam which is Bragg reflected from a crystalline layer of 2 μm thick on top of thick substrate. The layer and the substrate are both Si, reflection is (111). The lattice mismatch between the layer and the substrate is $\Delta d / d = D \times 10^{-4}$, the values of D are shown on the panels. The center of the angular aperture corresponds to the exact Bragg angle for the substrate.

this peak, as was discussed in the previous section, is a breakup of the destructive interference at the interface. With increasing D the reflectivity from the interface increases and the peak is getting sharper. At the same time, the peak from the layer is getting weaker which can be explained by a finite aperture of the lens. Indeed, the angular aperture of the lens can be estimated as $a_\gamma = A_\gamma / F \approx 100$ μrad FWHM while the shift of the Bragg angle for $D = 4$ is $\Delta \theta_B = 31.7$ μrad. With increasing D more x rays in the focused beam cannot satisfy Bragg condition for the layer and at $D = 10$ the peak from the layer almost disappears. The peak from the substrate for $D = 10$ shows a complex structure with additional oscillations which are the result of a complicated interference of reflected x rays with various paths lengths.

The interesting property of the proposed technique is that it is not sensitive to the sign of the deformation, i.e., the intensity distribution for $+D$ and $-D$ are exactly the same. It can be easily confirmed by the computer simulations and the physical explanation is as follows. The change of the sign of the deformation leads to a change of phases of the waves but not to a change of their amplitudes. The break of the destruc-
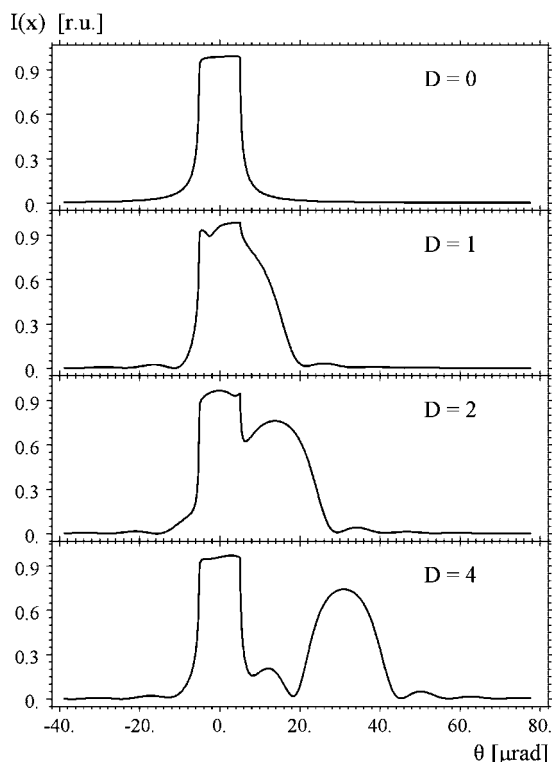
FIG. 5. X-ray rocking curves for the same sample as in Fig. 5 and the same values of the lattice mismatch except $D=10$.

tive interference is due to the phase difference, but it is not sensitive to a sign of this difference. However, the sign of the deformation can be revealed in experiment by rotating the crystal (see below).

In this respect, it is interesting to compare this technique with the well known high-resolution diffraction in which the angular dependence of the reflectivity of the plane wave (rocking curve) is measured. The rocking curves can be calculated by using formulas (6)–(9) and the result for the same values of D is shown in Fig. 5 (not shown is the curve for $D=10$ which is the same as for $D=4$ but with the layer peak shifted further away from the substrate peak). As one can see by comparing Figs. 4 and 5 the two techniques are mutually complementary. The narrow beam technique can directly determine the position of the interface inside the sample by measuring the distance between the edges of the two peaks and the accuracy of this measurement increases with the lattice mismatch (within the lens angular aperture). However, the value of $\Delta d/d$ cannot be measured directly but only through a fitting of the experimental intensity curve. On the contrary, the high-resolution diffraction technique shows immediately the lattice constant difference as the angular distance between two peaks, however, the thickness of the layer can only be obtained through the rocking curve fitting. The sensitivity of the both techniques are approximately the same.

Finally, we want to analyze the evolution of the intensity distribution with the thickness of the layer. As in the case of a standard x-ray topography, the spatial distribution depends on the angular position of the sample. We calculated the intensity patterns for the layers with the thickness from
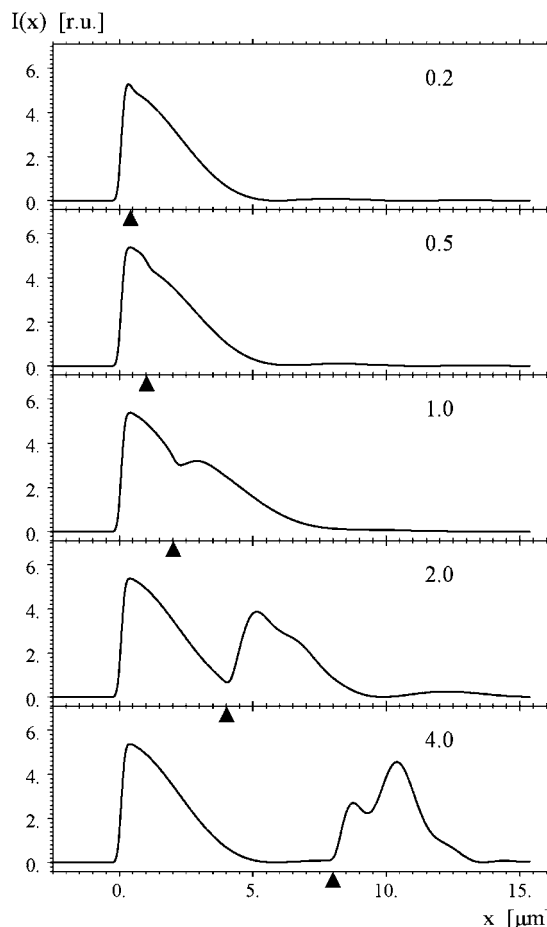

FIG. 6. Spatial relative intensity distribution of a focused beam which is Bragg reflected from a crystalline layer of different thickness on top of a thick substrate. The thickness of the layer is indicated on each panel. The calculations were performed for the lattice mismatch of $\Delta d/d=2\times10^{-4}$. The sample is oriented in such a way that the center of the angular aperture corresponds to the exact Bragg angle for the layer. Black triangles indicate the position of the interface.

0.2–4.0 μm and for the lattice mismatch $\Delta d/d=2\times10^{-4}$ (Fig. 6) and $\Delta d/d=10^{-3}$ (Fig. 7). The sample is assumed now to be rotated in such a way that the center of the angular aperture is at the exact Bragg angle for the layer. In both figures the spatial geometrical position of the interface at $x=x_0$ is marked by a black triangle. For the small lattice mismatch (see Fig. 6) the peak from the substrate is strong and it dominates the intensity patterns for the thin layers: the layer with the thickness of $t=0.2$ μm is too thin and cannot be observed under these conditions, the layer of $t=0.5$ μm thick manifests itself as a weak inflection point on a single peak, and only for the layer of 1 μm thick can the interface be clearly seen. For the layers with the thickness higher than the extinction length, $t=2$ and 4 μm, separate strong peaks from the layer and the substrate are observed. The situation is different for the higher mismatch of $\Delta d/d=10^{-3}$, Fig. 7. For this mismatch only a small part of the x rays from the incident beam can be diffracted from the substrate. Even for the thinnest layer of 0.2 μm thick a single kinematical peak from the layer is observed with the shape determined by the
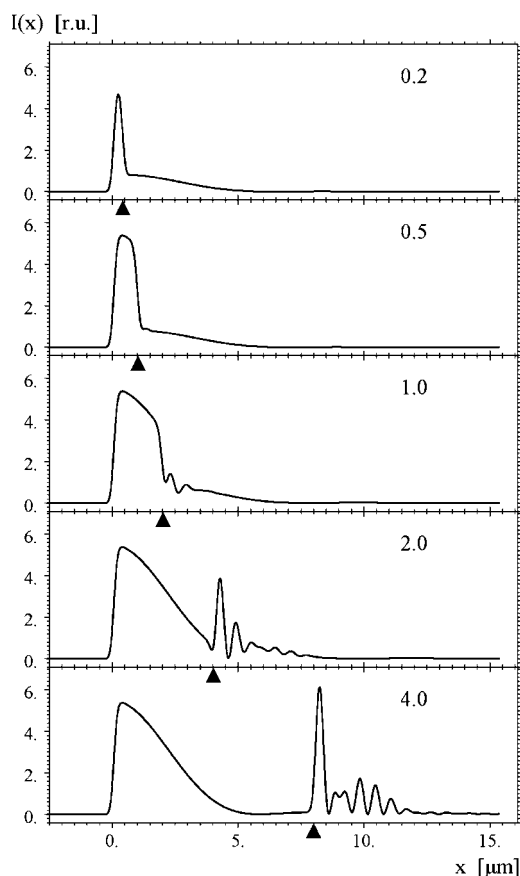
FIG. 7. The same curves as in the Fig. 6, but for the lattice mismatch of $\Delta d/d=10^{-3}$.

angular distribution of the incident beam. The intensity from the substrate is weak and broad. For the thicker layers of 0.5 and 1.0 μm the width of the reflected beam is proportional to the layer thickness and the intensity shows a sharp drop at the interface. For the thicker layers of 2.0 and 4.0 μm the dynamical diffraction takes place in the layer showing a gradual decrease of the intensity with x. As it becomes clear from these simulations the sign of the deformation can be determined by rotating the crystal and comparing intensity patterns taken at different angles within the angular aperture.

V. DISCUSSION AND CONCLUSION

Computer simulations presented in the previous sections demonstrate the extremely high sensitivity of a topographic technique based on a narrow focused beam to a spatial variation of a crystalline structure. For the multilayer crystal each interface can be recorded on intensity pattern. The interface may be an interface between layers of the same material with slightly different lattice constant due to strain, or between different crystalline materials, or between layers of the same material but different degree of crystalline perfection (static Debye-Waller factor). It can be shown that the thickness of the interface region also effects the intensity pattern. The contrast of the pattern and the sensitivity to individual layers depend on the angle of incidence. Thus, taking a series of

patterns at different angles can yield rich structural information about the sample.

The physical reason why we can see the interface, as discussed above, is due to a break-up of destructive interference in the bulk of the layer. It is obvious that a crystalline defect inside the layer may cause the same effect and can be visible on a recorded intensity pattern. One of the advantages of the proposed technique is the possibility of adjusting the field of view. By changing the position of the sample between the lens and detector one can zoom in and out on a particular region of the sample. The size of the smallest probed area is determined by geometrical restrictions of a particular experimental setup. We note here that the scheme in which the sample is positioned in the focus of the lens and the detector is placed at some distance behind the sample can be analyzed within the same theoretical approach though it is beyond the scope of this work.

It is also worth discussing requirements on the size of the focused beam. This question is related to the broadening of the focused beam due to diffraction and, ultimately, to the question of achievable depth resolution in a microdiffraction experiment. As one can see from the previous section the lateral size of the diffracted beam depends on the thickness of the probed layer. Only for layers with thickness of 0.2 μm and thinner is the size determined by the size of the focused beam (0.22 μm FWHM in our simulations). For thicker layers the smaller beam (say, ten times smaller, 20 nm, obtaining of which at present requires solving enormous technical problems) would yield basically the same pattern. The lateral size of the diffracted beam for these layers is determined by the thickness of the layer and, for layers with thickness close to or exceeding the extinction length for the chosen reflection, it is determined by the extinction length. Thus, the size of the beam should match the expected thickness of the thinnest layer or feature in the sample.

In conclusion, the optical scheme, in which a narrow beam produced by an x-ray focusing element, a parabolic refractive lens in this work, is Bragg reflected by a sample and the resulted intensity pattern is recorded at the focal point, is proposed. It constitutes an x-ray topographic technique with high sensitivity to the depth variations of the crystalline structure. Computer simulations were performed for a single layer and for the layer on top of a thick crystal, which is a common case for the epitaxially grown films. It was shown that the intensity contrast and the sensitivity of the method depends on the angle of incidence within the angular aperture of the lens. We may expect that the general properties of the proposed technique will also be present in other types of the focusing elements such as zone plates, KB mirrors, and others, though the details, of course, will be different (see comparison between a parabolic lens and a zone plate in Ref. 8).

*URL http://kohnvict.narod.ru

†ayk7@cornell.edu

[1] A. Autier, *Dynamical Theory of X-ray Diffraction* (Oxford University Press, Oxford, 2001).

[2] T. Uragami, J. Phys. Soc. Jpn. **27**, 147 (1969); **28**, 1508 (1970); **31**, 1141 (1971).

[3] A. M. Afanas'ev and V. G. Kohn, Acta Crystallogr., Sect. A: Cryst. Phys., Diffr., Theor. Gen. Crystallogr. **27**, 421 (1971).

[4] T. Saka, T. Katagawa, and N. Kato, Acta Crystallogr., Sect. A: Cryst. Phys., Diffr., Theor. Gen. Crystallogr. **28**, 102 (1972); **28**, 113 (1972); **29**, 192 (1973).

[5] A. Snigirev, V. Kohn, I. Snigireva, and B. Lengeler, Nature (London) **384**, 49 (1996).

[6] B. Lengeler, C. G. Schroer, M. Kuhlmann, B. Benner, T. F. Gunzler, O. Kurapova, F. Zontone, A. Snigirev, and I. Snigireva, J. Phys. D **38**, a218 (2005).

[7] V. Aristov, M. Grigoriev, S. Kuznetsov, L. Shabelnikov, V. Yunkin, C. Rau, A. Snigirev, I. Snigireva, T. Weitkamp, M. Hoffmann, and E. Voges, Nucl. Instrum. Methods Phys. Res. A **470**, 131 (2001).

[8] V. G. Kohn, Crystallogr. Rep. **51**, 564 (2006).

[9] S.-L. Chang, Yu. P. Stetsko, M.-T. Tang, Y.-R. Lee, W.-H. Sun, M. Yabashi, and T. Ishikawa, Phys. Rev. Lett. **94**, 174801 (2005).

[10] V. G. Kohn, JETP **97**, 204 (2003).

[11] V. G. Kohn, Yu. V. Shvydko, and E. Gerdau, Phys. Status Solidi B **221**, 597 (2000).

[12] URL http://java.sun.com

[13] URL http://vkacl.narod.ru

[14] V. G. Kohn, JETP Lett. **76**, 600 (2002).

[15] S. S. Yakimov, V. A. Chaplanov, A. M. Afanasev, P. A. Aleksandrov, R. M. Imamov, and L. A. Lomov, JETP Lett. **39**, 1 (1984).

[16] A. M. Afanasev, P. A. Aleksandrov, R. M. Imamov, L. A. Lomov, and A. A. Zavyalova, Acta Crystallogr., Sect. A: Found. Crystallogr. **A41**, 227 (1985).

[17] I. K. Robinson, Phys. Rev. B **33**, 3830 (1986).